

Distinct B cell subsets give rise to antigen-specific antibody responses against SARS-CoV-2

Christopher T. Stamper^{1,13}, Haley L. Dugan^{1,13}, Lei Li^{2,13}, Nicholas W. Asby³, Peter J. Halfmann⁴, Jenna J. Guthmiller², Nai-Ying Zheng², Min Huang², Olivia Stovicek², Jiaolong Wang², Maria Lucia Madariaga⁵, Kumaran Shanmugarajah⁵, Maud O. Jansen⁶, Fatima Amanat⁷, Isabelle Stewart^{2†}, Siriruk Changrob², Henry A. Utset², Jun Huang^{1,3}, Christopher A. Nelson⁸, Ya-Nan Dai⁸, Paige D. Hall⁸, Robert P. Jedrzejczak^{9,10}, Andrzej Joachimiak^{9,10,11}, Florian Krammer⁷, Daved H. Fremont⁸, Yoshihiro Kawaoka^{4,12}, Patrick C. Wilson^{1,2,14*}

Affiliations:

¹Committee on Immunology, University of Chicago, Chicago, IL 60637, USA.

²University of Chicago Department of Medicine, Section of Rheumatology, Chicago, IL 60637, USA.

³Pritzker School of Molecular Engineering, University of Chicago, Chicago, IL 60637, USA.

⁴Influenza Research Institute, Department of Pathobiological Sciences, School of Veterinary Medicine, University of Wisconsin-Madison, Madison, WI 53711, USA.

⁵University of Chicago Department of Surgery, Chicago, IL 60637, USA.

⁶University of Chicago Department of Medicine, Chicago, IL 60637, USA.

⁷Department of Microbiology, Icahn School of Medicine at Mount Sinai, New York, NY 10029, USA.

⁸Department of Pathology and Immunology, Washington University School of Medicine, St Louis, MO 63130, USA.

⁹Center for Structural Genomics of Infectious Diseases, Consortium for Advanced Science and Engineering, University of Chicago, Chicago, IL 60637, USA.

¹⁰Structural Biology Center, X-ray Science Division, Argonne National Laboratory, Lemont, IL 60439, USA.

¹¹Department of Biochemistry and Molecular Biology, University of Chicago, Chicago, IL 60637, USA.

¹²Division of Virology, Department of Microbiology and Immunology, Institute of Medical Science, University of Tokyo, 108-8639 Tokyo, Japan.

¹³These authors contributed equally.

¹⁴Lead Contact.

[†]Current address: School of Biological Sciences, Victoria University of Wellington, Wellington 6012, New Zealand.

*Correspondence: wilsonp@uchicago.edu (P.C.W.)

44 **Summary**

45 Discovery of durable memory B cell (MBC) subsets against neutralizing viral epitopes is critical for
46 determining immune correlates of protection from SARS-CoV-2 infection. Here, we identified
47 functionally distinct SARS-CoV-2-reactive B cell subsets by profiling the repertoire of convalescent
48 COVID-19 patients using a high-throughput B cell sorting and sequencing platform. Utilizing barcoded
49 SARS-CoV-2 antigen baits, we isolated thousands of B cells that segregated into discrete functional
50 subsets specific for the spike, nucleocapsid protein (NP), and open reading frame (ORF) proteins 7a and
51 8. Spike-specific B cells were enriched in canonical MBC clusters, and monoclonal antibodies (mAbs)
52 from these cells were potently neutralizing. By contrast, B cells specific to ORF8 and NP were enriched
53 in naïve and innate-like clusters, and mAbs against these targets were exclusively non-neutralizing.
54 Finally, we identified that B cell specificity, subset distribution, and affinity maturation were impacted by
55 clinical features such as age, sex, and symptom duration. Together, our data provide a comprehensive tool
56 for evaluating B cell immunity to SARS-CoV-2 infection or vaccination and highlight the complexity of
57 the human B cell response to SARS-CoV-2.

58

59

60

61

62

63

64

65

66

67

68

69

70

71

72

73

74

75 **Introduction**

76 Since the emergence of SARS-CoV-2 in December 2019, the World Health Organization has reported
77 spread to over 200 countries with infections approaching 30 million and deaths 1 million worldwide.
78 Despite this burden, the quest to identify effective vaccines, therapies, and protective biomarkers
79 continues. The isolation of human monoclonal antibodies (mAbs) specific for immunogenic SARS-CoV-
80 2 proteins holds immense potential, as they can be rapidly employed as therapeutic agents, diagnostic
81 reagents, and aid vaccine optimization. Several independent groups have identified potently neutralizing
82 mAbs against the SARS-CoV-2 spike protein, the major immunogenic surface glycoprotein¹⁻⁷. Despite
83 these advances, there have been no mAbs isolated against other immunogenic targets of SARS-CoV-2,
84 including the internal nucleoprotein (NP) and open reading frame (ORF) proteins 7 and 8, which have
85 been suggested to induce antibody responses and immunomodulatory effects in humans⁸⁻¹². Moreover, the
86 properties and frequencies of B cell subsets targeting distinct SARS-CoV-2 antigens remain poorly
87 understood, and are likely shaped by clinical features such as age and disease severity^{6,13,14}.

88
89 To address these knowledge gaps, we comprehensively characterized the SARS-CoV-2-specific B cell
90 repertoire in convalescent COVID-19 patients and generated mAbs against the spike, ORF8, and NP
91 proteins. Together, our data reveal key insight into antigen specificity and B cell subset distribution upon
92 SARS-CoV-2 infection in the context of age, sex, and disease severity.

93
94 **Results**

95 **SARS-CoV-2-specific B cell sequencing**

96 Serum antibodies and MBCs have potential to act as the first line of defense against SARS-CoV-2
97 infection^{11,15-17}. To determine the landscape of antibody reactivity toward distinct SARS-CoV-2 viral
98 targets, we collected peripheral blood mononuclear cells (PBMCs) and serum from 25 subjects between
99 April and May of 2020 upon recovery from SARS-CoV-2 viral infection (Extended Data Table 1 and
100 Extended Data Table 2). To identify B cells specific to the SARS-CoV-2 spike protein, spike RBD,
101 ORF7a, ORF8, and NP, we generated probes to bait-sort enriched B cells for subsequent single cell RNA
102 sequencing analysis by conjugating distinct phycoerythrin (PE)-streptavidin (SA)-oligos to individual
103 biotinylated antigens (Fig. 1a).

104
105 From 25 subjects analyzed, we detected small percentages (0.02–0.26%) of SARS-CoV-2-reactive total
106 CD19⁺ B cells, which were subsequently used to prepare 5' transcriptome, immunoglobulin (Ig) VDJ, and

107 antigen-specific probe feature libraries for sequencing (Fig. 1a, b). We detected increased percentages of
108 antigen-specific B cells within the memory B cell (MBC) compartment (Fig. 1b, CD19⁺CD27⁺CD38^{int}),
109 though we sorted on total CD19⁺ antigen-specific B cells to ensure adequate coverage of all potential
110 reactive B cells and to optimize sequence library preparation and downstream analysis as the antigen-
111 specific population was rare. We integrated data from 17 subjects with high-quality sequencing results
112 using Seurat to remove batch effects and identified 12 transcriptionally distinct B cell clusters based on
113 transcriptional expression profiles (Fig. 1c). It was immediately evident that B cells specific to the spike,
114 NP, and ORF8 were found amongst multiple B cell subsets, with spike-specific B cells substantially
115 enriched in clusters 4, 5, 7, and 9 (Fig. 1d, e). Analysis of Ig isotypes and degree of Ig variable heavy
116 chain somatic hypermutations (VH SHM) suggested that clusters 0–2, 8, 10, and 11 represented naïve- or
117 innate-like B cell clusters predominantly composed of IgM and IgD B cells. In contrast, clusters 3, 4, 5,
118 6, 7, 9, and 12 strongly indicated B cell subsets more similar to MBCs or plasma cells, as they exhibited
119 a higher degree of class switch recombination (CSR) and/or increased numbers of VH SHM (Fig. 1f). We
120 detected variation in the percentage of total cells sorted per cluster amongst individual patients, reflecting
121 differences in the biology of individual responses to SARS-CoV-2, as we expand upon later (Extended
122 Data Fig. 1a). No major differences in VH gene usage across clusters were evident, though we identified
123 enrichment of VH1-24 in cluster 7, which we later identify as exclusively utilized by spike-reactive B
124 cells (Extended Data Fig. 1b).

125
126 We next addressed whether the probe intensities generated from our feature libraries correlated with
127 antigen-specific reactivity by plotting intensities for distinct probes against one another to observe true
128 specificity (cells that fall directly onto the x or y axis) vs. non-specific binding (cells that fall on the
129 diagonal). We observed hundreds of cells specific to the spike, ORF8, and NP, and to a lesser degree, the
130 RBD alone and ORF7a (Fig. 1g). For clusters 0, 1, 2, and 8, we observed that the majority of cells were
131 not uniquely specific for any one probe, and instead tended to bind more than one probe in a polyreactive
132 or non-specific manner, consistent with innate-like B cells¹⁸. Finally, clusters 4, 5, 6, 7, and 9 exhibited
133 highly specific binding toward the spike, NP, and ORF8, with the majority targeting the spike (Extended
134 Data Fig. 1c). Together, our data suggest the B cell response to SARS-CoV-2 is comprised of multiple
135 functionally distinct B cell subsets enriched for binding to distinct viral targets.

136

137

138 **SARS-CoV-2-specific B cell subsets**

139 To discern the identities of distinct B cell subsets, we further analyzed Ig repertoire, differentially
140 expressed genes, and performed pseudotime analyses of integrated clusters. For pseudotime analysis, we
141 rooted the data on cluster 2, as cells within this cluster expressed Ig genes with little to no SHM or CSR
142 (Fig. 1f) and displayed low probe reactivity (Extended Data Fig. 1c), suggesting this subset is comprised
143 of true naïve B cells. Pseudotime analysis rooted on cluster 2 identified clusters 0, 1, and 8 in various
144 stages of differentiation, suggestive of recent activation (Fig. 2a–b). As they displayed little CSR or SHM
145 (Fig. 1f), we therefore categorized these subsets as innate-like or possibly germinal center independent.
146 Clusters 3 and 5 appeared to be specific IgM memory subsets (Fig. 1f and Extended Data Fig. 1c), while
147 clusters 4, 7, 9, and 12 displayed high specificity, CSR, and SHM, demonstrating an affinity-matured
148 memory phenotype (Fig. 1f and Extended Data Fig. 1c). As naïve B cells and MBCs are quiescent, clusters
149 4, 5, 7, and 9 were similar to cluster 2 in pseudotime analysis (Fig. 2a–b)¹⁹. Lastly, cluster 6 was of interest
150 as these cells displayed the greatest frequency of SHM and IgA CSR, and may have arisen in the context
151 of a mucosal immune response.

152
153 In-depth analysis of select genes including those related to B cell fate, MBC differentiation and
154 maintenance, and long-lived plasma cells (LLPCs) helped to further reveal the identities of select clusters.
155 Genes associated with MBCs (*cd27*, *cd38*, *cd86*, *pou2af*), repression of apoptosis (*mcl1*), early
156 commitment to B cell fate (*zeb2*), repression of LLPC fate (*spiB*, *pax5*, *bach2*), and early B cell activation
157 and proliferation (*bach2*) confirmed clusters 3, 4, 5, 7 and 9 as MBCs though with varying degrees of
158 differentiation, CSR, and SHM (Fig 2b–c and Extended Data Fig 2). Notably, we identified upregulation
159 of the transcription factor *hhex* in cluster 7, which has recently been shown to be involved in MBC
160 differentiation in mice (Extended Data Fig. 2)²⁰. Lastly, cluster 12 appeared to be LLPCs or precursors
161 thereof by expression of genes associated with LLPC fate, including *prdm1*, *xbp1*, and *manf* (Extended
162 Data Fig. 2)^{19,21,22}. Together with our antigen-specific probe data (Fig. 1), these results confirm that
163 clusters representing classical MBCs are enriched for spike binding while B cells targeting internal
164 proteins are enriched in activated naïve and innate-like B cell subsets.

165
166 **SARS-CoV-2-specific Ig repertoire**

167 The properties of B cells targeting immunogenic targets such as ORF8 and NP compared to the spike are
168 unknown. We further analyzed isotype frequencies, VH SHM, VH gene usages, and frequencies of B cells
169 against these targets within distinct B cell subsets. The majority of antigen-specific B cells were of the

170 IgM isotype with a limited degree of CSR. There were no major differences between the isotypes of B
171 cells specific to these distinct targets, with the majority of class-switched cells being of the IgG1 isotype.
172 Consistent with a *de novo* response against the novel SARS-CoV-2, we observed that the majority of
173 antigen-specific B cells had little to no VH SHM, though spike-reactive B cells displayed slightly
174 increased amounts of SHM. Spike-specific B cells were primarily enriched in MBC and LLPC-like
175 clusters 4, 5, 7, 9, and 12 while NP- and ORF8-specific B cells were largely found within naïve- and
176 innate-like clusters but also within MBC clusters (Fig. 3a–l). Lastly, we did not observe differences in
177 heavy chain (HC) or light chain (LC) complementarity determining region 3 length by antigen targeting
178 (Extended Data Fig. 3a–b), though we did observe that HC and LC isoelectric points (pI) for spike-reactive
179 B cells were generally lower than NP- or ORF8-reactive B cells (Extended Data Fig. 3c–d), and LC SHM
180 was greater for spike-reactive B cells (Extended Data Fig. 3e).

181
182 We next analyzed the VH gene usages of spike-, NP-, and ORF8-specific B cells and identified the most
183 common VH usages per reactivity (represented by larger squares on each tree map) as well as shared VH
184 usages across reactivities (shown by matching colors; Fig. 3m–p). Strikingly, we identified usage of
185 particular VH gene loci that did not overlap between spike- and RBD-reactive B cells (shown in black).
186 VH1-24, VH3-7, and VH3-9 were the highest represented VH gene usages exclusively associated with
187 non-RBD spike reactivity, and VH1-24 usage was enriched in cluster 7, an MBC-like cluster (Fig. 3m–n
188 and Extended Data Fig. 1b). These results were confirmed by mAb data, which identified spike-specific
189 mAbs utilizing VH1-24 and VH3-7 that did not bind to the RBD (Extended Data Table 3). Unique LC V
190 gene usages were also evident amongst antigen-specific cells (Extended Data Fig. 3f–i).

191
192 Finally, public B cell clones were of interest as the epitopes bound can be targeted by multiple people and
193 thus represent important vaccine targets. We identified five novel public clones from this dataset, three of
194 which were present in two separate subjects, one that was present amongst three subjects, and one amongst
195 four subjects (Extended Data Table 4). Four of the clonal pools were specific to the spike protein, and the
196 remaining clone to NP. The majority of clonal pool members were identified in MBC-like clusters 3, 4,
197 5, 7, and 9, suggesting that B cells specific to public epitopes can be established within stable MBC
198 compartments.

199

200 **Monoclonal antibody binding and neutralization**

201 To simultaneously validate the specificity of our approach and investigate the properties of mAbs targeting
202 distinct SARS-CoV-2 viral epitopes, we synthesized and characterized the binding and neutralization
203 ability of 90 mAbs from our single cell dataset (Extended Data Table 3). B cells exhibiting variable probe
204 binding intensities toward distinct antigens were chosen as candidates for mAb generation, as well as B
205 cells that tended to bind multiple probes (exhibiting non-specificity or polyreactivity). MAbs cloned were
206 representative of various clusters, reactivities, VH gene usages, mutational load, and isotype usages (Fig.
207 4a, Extended Data Table 3). Representative mAbs generated from cells specific to the spike, NP, and
208 ORF8 exhibited high affinity by ELISA, though probe intensities did not meaningfully correlate with
209 apparent affinity (K_D) (Fig. 4b, Extended Data Fig. 4a). Only a small percentage of cloned mAbs to the
210 spike, NP, and ORF8 exhibited non-specific binding (Fig. 4b). Notably, cells exhibiting non-specific
211 binding were reactive to the PE-SA-oligo probe conjugate and were largely polyreactive (Extended Data
212 Fig. 4b–g).

213
214 While mAbs targeting the RBD of the spike are typically neutralizing, little is known regarding the
215 neutralization capabilities of mAbs targeting non-RBD regions of the spike, ORF8 and NP. We addressed
216 the neutralization ability of all synthesized mAbs using a live virus plaque assay and determined that all
217 mAbs cloned against NP and ORF8 were non-neutralizing, while mAbs against the RBD and other
218 epitopes of the spike were largely neutralizing at varying degrees of potency (Fig. 4c–d). As anti-spike
219 mAbs were predominantly neutralizing and enriched in memory, these MBC subsets may serve as a
220 biomarker for superior immunity to SARS-CoV-2.

221 222 **Antigen targeting and clinical features**

223 Previous studies from our group and others have suggested serum antibody titers correlate with sex,
224 SARS-CoV-2 severity, and age^{6,14,23}. We therefore investigated the frequencies of SARS-CoV-2-reactive
225 B cells to assess whether reactivity toward particular SARS-CoV-2 antigens correlated with clinical
226 parameters. By both serology and ELISpot, we identified that B cell responses against the spike/RBD and
227 NP were immunodominant, though ORF8 antigen targeting was substantial (Fig. 5a, b). Consistent with
228 our single cell dataset, spike-specific B cells were enriched in memory by ELISpot (Fig. 5b).

229
230 We next analyzed the distribution of B cell subsets and frequencies of B cells specific to the spike, NP,
231 ORF7a, and ORF8 in sets of patients stratified by age, sex, and duration of symptoms from our single cell
232 dataset. We normalized antigen probe signals by a centered log-ratio transformation individually for each

233 subject; all B cells were clustered into multiple probe hit groups according to their normalized probe
234 signals, and cells that were negative to all probes or positive to all probes (non-specific) were excluded
235 from the analysis. We identified substantial variation amongst individual subjects in terms of the degree
236 of spike, NP, ORF7a, and ORF8 antigen targeting (Fig. 5c). As subject age increased, the percentages of
237 spike-reactive B cells relative to B cells targeting internal proteins decreased, and age positively correlated
238 with increased percentages of ORF8-reactive B cells (Fig. 5d–e). Similarly, female subjects and subjects
239 experiencing a longer duration of symptoms displayed reduced spike targeting relative to internal proteins
240 (Fig. 5d). Consistent with spike-reactive B cells enriched in MBC clusters, patient who were younger,
241 male, or experienced a shorter duration of symptoms exhibited increased targeting of the spike and
242 increased proportions of MBC subsets (Fig. 5d, f). Accordingly, older patients, female patients, and
243 patients with a longer duration of symptoms exhibited reduced levels of VH gene SHM (Fig. 5g–i).

244
245 In summary, our study highlights the diversity of B cell subsets expanded upon novel infection with
246 SARS-CoV-2. Using this approach, we identified that B cells against the spike, ORF8, and NP differ in
247 their ability to neutralize, derive from functionally distinct and differentially adapted B cell subsets, and
248 correlate with clinical parameters such as age, sex, and symptom duration.

249 **Discussion**

251 The COVID-19 pandemic continues to pose one of the greatest public health and policy challenges in
252 modern history, and robust data on long-term immunity is critically needed to evaluate future decisions
253 regarding COVID-19 responses. Our approach combines three powerful aspects of B cell biology to
254 address human immunity to SARS-CoV-2: B cell transcriptome, Ig sequencing, and recombinant mAb
255 characterization. Our approach enables the identification of potentially neutralizing antibodies and the
256 characteristics of the B cells that generate them. Importantly, we showed that antibodies targeting key
257 protective spike epitopes are enriched within canonical MBC populations.

258
259 Identification of multiple distinct subsets of innate-like B cells, MBCs, and apparent LLPC precursors
260 illustrates the complexity of the B cell response to SARS-CoV-2, revealing an important feature of the
261 immune response against a novel pathogen. The B cell clusters herein may provide biomarkers in the form
262 of distinct B cell populations that can be used to evaluate future responses to various vaccine formulations.
263 In particular, the identification of LLPC precursors in the blood following infection and vaccination has
264 been long sought after, as they serve as a bonafide marker of long-lived immunity^{24,25}. Future studies

265 elucidating distinct identities and functions of these subsets are necessary and will provide key insights
266 into B cell immunology.

267
268 We identified that older patients, female patients, and patients experiencing a longer duration of symptoms
269 tended to display reduced proportions of MBC clusters and reduced VH SHM, consistent with a previous
270 study that identified limited germinal center formation upon SARS-CoV-2 infection²⁶. Notably, older
271 patients had increased percentages of ORF8-specific B cells, which we identified as exclusively non-
272 neutralizing. Mechanistically, these observations may be explained by reduced adaptability of B cells or
273 increased reliance on CD4 T cell help for B cell activation, which have been observed in aged individuals
274 upon viral infections^{27,28}. Furthermore, T cell responses to SARS-CoV-2 ORF proteins are prevalent in
275 convalescent COVID-19 patients, and recent studies suggest impaired T cell responses in aged COVID-
276 19 patients impact antibody responses^{10,29,30,42}. More research is warranted to definitively determine
277 whether B cell targeting of distinct SARS-CoV-2 antigens correlates with age and disease severity.
278 Addressing these questions will be critical for determining correlates of protection and developing a
279 vaccine capable of protecting our most vulnerable populations.

280

281 **Bibliography**

- 282 1 Chen, X. *et al.* Human monoclonal antibodies block the binding of SARS-CoV-2 spike protein to
283 angiotensin converting enzyme 2 receptor. *Cell Mol Immunol* **17**, 647-649, doi:10.1038/s41423-
284 020-0426-7 (2020).
- 285 2 Wang, C. *et al.* A human monoclonal antibody blocking SARS-CoV-2 infection. *Nat Commun* **11**,
286 2251, doi:10.1038/s41467-020-16256-y (2020).
- 287 3 Yi, C. *et al.* Key residues of the receptor binding motif in the spike protein of SARS-CoV-2 that
288 interact with ACE2 and neutralizing antibodies. *Cell Mol Immunol* **17**, 621-630,
289 doi:10.1038/s41423-020-0458-z (2020).
- 290 4 Lan, J. *et al.* Structure of the SARS-CoV-2 spike receptor-binding domain bound to the ACE2
291 receptor. *Nature* **581**, 215-220, doi:10.1038/s41586-020-2180-5 (2020).
- 292 5 Yan, R. *et al.* Structural basis for the recognition of SARS-CoV-2 by full-length human ACE2.
293 *Science* **367**, 1444-1448, doi:10.1126/science.abb2762 (2020).
- 294 6 Robbiani, D. F. *et al.* Convergent antibody responses to SARS-CoV-2 in convalescent individuals.
295 *Nature* **584**, 437-442, doi:10.1038/s41586-020-2456-9 (2020).
- 296 7 Wec, A. Z. *et al.* Broad neutralization of SARS-related viruses by human monoclonal antibodies.
297 *Science* **369**, 731-736, doi:10.1126/science.abc7424 (2020).
- 298 8 Kopecky-Bromberg, S. A., Martinez-Sobrido, L., Frieman, M., Baric, R. A. & Palese, P. Severe
299 acute respiratory syndrome coronavirus open reading frame (ORF) 3b, ORF 6, and nucleocapsid
300 proteins function as interferon antagonists. *J Virol* **81**, 548-557, doi:10.1128/JVI.01782-06
301 (2007).

302 9 Lu, X., Pan, J., Tao, J. & Guo, D. SARS-CoV nucleocapsid protein antagonizes IFN-beta response
303 by targeting initial step of IFN-beta induction pathway, and its C-terminal region is critical for
304 the antagonism. *Virus Genes* **42**, 37-45, doi:10.1007/s11262-010-0544-x (2011).

305 10 Grifoni, A. *et al.* Targets of T Cell Responses to SARS-CoV-2 Coronavirus in Humans with COVID-
306 19 Disease and Unexposed Individuals. *Cell* **181**, 1489-1501 e1415,
307 doi:10.1016/j.cell.2020.05.015 (2020).

308 11 Ni, L. *et al.* Detection of SARS-CoV-2-Specific Humoral and Cellular Immunity in COVID-19
309 Convalescent Individuals. *Immunity* **52**, 971-977 e973, doi:10.1016/j.immuni.2020.04.023
310 (2020).

311 12 Li, J. Y. *et al.* The ORF6, ORF8 and nucleocapsid proteins of SARS-CoV-2 inhibit type I interferon
312 signaling pathway. *Virus Res* **286**, 198074, doi:10.1016/j.virusres.2020.198074 (2020).

313 13 Atyeo, C. *et al.* Distinct Early Serological Signatures Track with SARS-CoV-2 Survival. *Immunity*
314 **53**, 524-532 e524, doi:10.1016/j.immuni.2020.07.020 (2020).

315 14 Guthmiller, J. J. *et al.* SARS-CoV-2 infection severity is linked to superior humoral immunity
316 against the spike. *bioRxiv*, doi:10.1101/2020.09.12.294066 (2020).

317 15 Brouwer, P. J. M. *et al.* Potent neutralizing antibodies from COVID-19 patients define multiple
318 targets of vulnerability. *Science*, doi:10.1126/science.abc5902 (2020).

319 16 Cao, Y. *et al.* Potent Neutralizing Antibodies against SARS-CoV-2 Identified by High-Throughput
320 Single-Cell Sequencing of Convalescent Patients' B Cells. *Cell* **182**, 73-84 e16,
321 doi:10.1016/j.cell.2020.05.025 (2020).

322 17 Hansen, J. *et al.* Studies in humanized mice and convalescent humans yield a SARS-CoV-2
323 antibody cocktail. *Science*, doi:10.1126/science.abd0827 (2020).

324 18 Zhang, X. Regulatory functions of innate-like B cells. *Cell Mol Immunol* **10**, 113-121,
325 doi:10.1038/cmi.2012.63 (2013).

326 19 Palm, A. E. & Henry, C. Remembrance of Things Past: Long-Term B Cell Memory After Infection
327 and Vaccination. *Front Immunol* **10**, 1787, doi:10.3389/fimmu.2019.01787 (2019).

328 20 Laidlaw, B. J., Duan, L., Xu, Y., Vazquez, S. E. & Cyster, J. G. The transcription factor Hhex
329 cooperates with the corepressor Tle3 to promote memory B cell development. *Nat Immunol* **21**,
330 1082-1093, doi:10.1038/s41590-020-0713-6 (2020).

331 21 Lightman, S. M., Utley, A. & Lee, K. P. Survival of Long-Lived Plasma Cells (LLPC): Piecing
332 Together the Puzzle. *Front Immunol* **10**, 965, doi:10.3389/fimmu.2019.00965 (2019).

333 22 Brynjolfsson, S. F. *et al.* Long-Lived Plasma Cells in Mice and Men. *Front Immunol* **9**, 2673,
334 doi:10.3389/fimmu.2018.02673 (2018).

335 23 Atyeo, C. *et al.* Distinct Early Serological Signatures Track with SARS-CoV-2 Survival. *Immunity*,
336 doi:10.1016/j.immuni.2020.07.020 (2020).

337 24 Garimalla, S. *et al.* Differential transcriptome and development of human peripheral plasma cell
338 subsets. *JCI Insight* **4**, doi:10.1172/jci.insight.126732 (2019).

339 25 Lau, D. *et al.* Low CD21 expression defines a population of recent germinal center graduates
340 primed for plasma cell differentiation. *Sci Immunol* **2**, doi:10.1126/sciimmunol.aai8153 (2017).

341 26 Kaneko, N. *et al.* Loss of Bcl-6-Expressing T Follicular Helper Cells and Germinal Centers in
342 COVID-19. *Cell*, doi:10.1016/j.cell.2020.08.025 (2020).

343 27 Dugan, H. L., Henry, C. & Wilson, P. C. Aging and influenza vaccine-induced immunity. *Cell*
344 *Immunol* **348**, 103998, doi:10.1016/j.cellimm.2019.103998 (2020).

345 28 Henry, C. *et al.* Influenza Virus Vaccination Elicits Poorly Adapted B Cell Responses in Elderly
346 Individuals. *Cell Host Microbe* **25**, 357-366 e356, doi:10.1016/j.chom.2019.01.002 (2019).
347 29 Le Bert, N. *et al.* SARS-CoV-2-specific T cell immunity in cases of COVID-19 and SARS, and
348 uninfected controls. *Nature* **584**, 457-462, doi:10.1038/s41586-020-2550-z (2020).
349 30 Peng, Y. *et al.* Broad and strong memory CD4(+) and CD8(+) T cells induced by SARS-CoV-2 in UK
350 convalescent individuals following COVID-19. *Nat Immunol*, doi:10.1038/s41590-020-0782-6
351 (2020).
352 31 Amanat, F. *et al.* A serological assay to detect SARS-CoV-2 seroconversion in humans. *medRxiv*,
353 doi:10.1101/2020.03.17.20037713 (2020).
354 32 Stadlbauer, D. *et al.* SARS-CoV-2 Seroconversion in Humans: A Detailed Protocol for a
355 Serological Assay, Antigen Production, and Test Setup. *Curr Protoc Microbiol* **57**, e100,
356 doi:10.1002/cpmc.100 (2020).
357 33 Nelson, C. A., Pekosz, A., Lee, C. A., Diamond, M. S. & Fremont, D. H. Structure and intracellular
358 targeting of the SARS-coronavirus Orf7a accessory protein. *Structure* **13**, 75-85,
359 doi:10.1016/j.str.2004.10.010 (2005).
360 34 Nelson, C. A., Lee, C. A. & Fremont, D. H. Oxidative refolding from inclusion bodies. *Methods*
361 *Mol Biol* **1140**, 145-157, doi:10.1007/978-1-4939-0354-2_11 (2014).
362 35 Cao, J. *et al.* The single-cell transcriptional landscape of mammalian organogenesis. *Nature* **566**,
363 496-502, doi:10.1038/s41586-019-0969-x (2019).
364 36 Qiu, X. *et al.* Reversed graph embedding resolves complex single-cell trajectories. *Nat Methods*
365 **14**, 979-982, doi:10.1038/nmeth.4402 (2017).
366 37 Stuart, T. *et al.* Comprehensive Integration of Single-Cell Data. *Cell* **177**, 1888-1902 e1821,
367 doi:10.1016/j.cell.2019.05.031 (2019).
368 38 Guthmiller, J. J., Dugan, H. L., Neu, K. E., Lan, L. Y. & Wilson, P. C. An Efficient Method to
369 Generate Monoclonal Antibodies from Human B Cells. *Methods Mol Biol* **1904**, 109-145,
370 doi:10.1007/978-1-4939-8958-4_5 (2019).
371 39 Andrews, S. F. *et al.* Immune history profoundly affects broadly protective B cell responses to
372 influenza. *Sci Transl Med* **7**, 316ra192, doi:10.1126/scitranslmed.aad0522 (2015).
373 40 Bunker, J. J. *et al.* Natural polyreactive IgA antibodies coat the intestinal microbiota. *Science*
374 **358**, doi:10.1126/science.aan6619 (2017).
375 41 Shlomchik, M. J., Aucoin, A. H., Pisetsky, D. S. & Weigert, M. G. Structure and function of anti-
376 DNA autoantibodies derived from a single autoimmune mouse. *Proc Natl Acad Sci U S A* **84**,
377 9150-9154, doi:10.1073/pnas.84.24.9150 (1987).
378 42 Rydzynski Moderbacher, C. *et al.* Antigen-specific adaptive immunity to SARS-CoV-2 in acute
379 COVID-19 and associations with age and disease severity. *Cell* doi:10.1016/j.cell.2020.09.038
380 (2020).
381
382
383
384
385
386

387 **Materials & Methods**

388 **Study cohort and sample collection**

389 All studies were performed with the approval of the University of Chicago institutional review board
390 IRB20-0523 and University of Wisconsin-Madison institutional biosafety committees. Informed consent
391 was obtained after the research applications and possible consequences of the studies were disclosed to
392 study subjects. This clinical trial was registered at ClinicalTrials.gov with identifier NCT04340050, and
393 clinical information for patients included in the study is detailed in Extended Data Table 1 and Extended
394 Data Table 2. Leukoreduction filter donors were 18 years of age or older, eligible to donate blood as per
395 standard University of Chicago Medicine Blood Donation Center guidelines, had a documented COVID-
396 19 polymerase chain reaction (PCR) positive test, and complete resolution of symptoms at least 28 days
397 prior to donation. PBMCs were collected from leukoreduction filters within 2 hours post-collection and
398 flushed from the filters using sterile 1X Phosphate-Buffered Saline (PBS, Gibco) supplemented with 0.2%
399 Bovine Serum Albumin (BSA, Sigma). Lymphocytes were purified by Lymphoprep Ficoll gradient
400 (Thermo Fisher) and contaminating red blood cells were lysed by ACK buffer (Thermo Fisher). Cells
401 were frozen in Fetal Bovine Serum (FBS, Gibco) with 10% Dimethyl sulfoxide (DMSO, Sigma) prior to
402 downstream analysis. On the day of sorting, B cells were enriched using the human pan B cell EasySep™
403 enrichment kit (STEMCELL).

404

405 **Recombinant proteins and probe generation**

406 SARS-CoV-2 proteins were obtained from the Krammer laboratory at Mt. Sinai, the Joachimiak
407 laboratory at Argonne, and the Fremont laboratory at Washington University. pCAGGS expression
408 constructs for the spike protein and spike RBD were obtained from the Krammer lab at Mt. Sinai and
409 produced in house in Expi293F suspension cells (Thermo Fisher). Sequences for the spike and RBD
410 proteins as well as details regarding their expression and purification have been previously
411 described^{31,32}. Proteins were biotinylated for 2 hours on ice using EZ-Link™ Sulfo-NHS-Biotin, No-
412 Weigh™ Format (Thermo Fisher) according to the manufacturer's instructions, unless previously Avi-
413 tagged and biotinylated (ORF7a and ORF8 proteins, Fremont laboratory). Truncated cDNAs encoding
414 the Ig-like domains of ORF7a and ORF8 were inserted into the bacterial expression vector pET-21(a) in
415 frame with a biotin ligase recognition sequence at the c-terminus (GLNDIFEAQKIEWHE). Soluble
416 recombinant proteins were produced as described previously³³. In brief, inclusion body proteins were
417 washed, denatured, reduced, and then renatured by rapid dilution following standard methods³⁴. The

418 refolding buffer consisted of 400 mM arginine, 100 mM Tris-HCl, 2 mM EDTA, 200 μ M ABESF, 5
419 mM reduced glutathione, and 500 μ M oxidized glutathione at a final pH of 8.3. After 24 hours, the
420 soluble-refolded protein was collected over a 10 kDa ultrafiltration disc (EMD Millipore, PLGC07610)
421 in a stirred cell concentrator and subjected to chromatography on a HiLoad 26/60 Superdex S75 column
422 (GE Healthcare). Site-specific biotinylation with BirA enzyme was done following the manufacture's
423 protocol (Avidity) except that the reaction buffer consisted of 100mM Tris-HCl (pH 7.5) 150 mM NaCl,
424 with 5 mM MgCl₂ in place of 0.5 M Bicine at pH 8.3. Unreacted biotin was removed by passage
425 through a 7K MWCO desalting column (Zeba spin, Thermo Fisher). Full-length SARS-CoV-2 NP was
426 cloned into pET21a with a hexahistidine tag and expressed using BL21(DE3)-RIL *E. coli* in Terrific
427 Broth (bioWORLD). Following overnight induction at 25°C, cells were lysed in 20 mM Tris-HCl pH
428 8.5, 1 M NaCl, 5 mM β -mercaptoethanol, and 5 mM imidazole for nickel-affinity purification and size
429 exclusion chromatography. Biotinylated proteins were then conjugated to Biolegend TotalSeq™ PE
430 streptavidin- (PE-SA) oligos at a 0.72:1 molar ratio of antigen to PE-SA. The amount of antigen was
431 chosen based on a fixed amount of 0.5 μ g PE-SA and diluted in a final volume of 10 μ L. PE-SA was
432 then added gradually to 10 μ l biotinylated proteins 5 times on ice, 1 μ l PE-SA (0.1 mg/ml stock) every
433 20 minutes for a total of 5 μ l (0.5 μ g) PE-SA. The reaction was then quenched with 5 μ l 4mM Pierce™
434 biotin (Thermo Fisher) for 30 minutes for a total probe volume of 20 μ L. Probes were then used
435 immediately for staining.

436

437 **Antigen-specific B cell sorting**

438 PBMCs were thawed and B cells were enriched using EasySep™ pan B cell magnetic enrichment kit
439 (STEMCELL). B cells were stained with a panel containing CD19 PE-Cy7 (Biolegend), IgM APC
440 (Southern Biotech), CD27 BV605 (Biolegend), CD38 BB515 (BD Biosciences), and CD3 BV510 (BD
441 Biosciences). B cells were stained with surface stain master mix and each COVID-19 antigen probe for
442 30 minutes on ice in 1X PBS supplemented with 0.2% BSA and 2 mM Pierce Biotin. Cells were stained
443 with probe at a 1:100 dilution (NP, ORF7a, ORF8, RBD) or 1:200 dilution (spike). Cells were
444 subsequently washed with 1X PBS 0.2% BSA and stained with Live/Dead BV510 (Thermo Fisher) in 1X
445 PBS for 15 minutes. Cells were washed again and re-suspended at a maximum of 4 million cells/mL in
446 1X PBS supplemented with 0.2% BSA and 2 mM Pierce Biotin for downstream cell sorting using the
447 MACSQuantTyto cartridge sorting platform (Miltenyi). Cells that were viable/CD19⁺/antigen-PE⁺ were

448 sorted as probe positive. The PE⁺ gate was drawn by use of FMO controls. Cells were then collected from
449 the cartridge sorting chamber and used for downstream 10X Genomics analysis.

450
451 **10X Genomics library construction**

452 VDJ, 5', and probe feature libraries were prepared using the 10X Chromium System (10X Genomics,
453 Pleasanton, CA). The Chromium Single Cell 5' Library and Gel Bead v2 Kit, Human B Cell V(D)J
454 Enrichment Kit, and Feature Barcode Library Kit were used. All steps were followed as listed in the
455 manufacturer's instructions. Specifically, user guide CG000186 Rev D was used. Final libraries were
456 pooled and sequenced using the NextSeq550 (Illumina, San Diego, CA) with 26 cycles apportioned for
457 read 1, 8 cycles for the i7 index, and 134 cycles for read 2.

458
459 **Computational analyses for single cell sequencing data**

460 We adopted Cell Ranger (version 3.0.2) for raw sequencing processing, including 5' gene expression
461 analysis, antigen probe analysis, and immunoprofiling analysis of B cells. Based on Cell Ranger output,
462 we performed downstream analysis using Seurat (version 3.2.0, an R package, for transcriptome, cell
463 surface protein and antigen probe analysis) and IgBlast (version 1.15, for immunoglobulin gene analysis).
464 For transcriptome analysis, Seurat was used for cell quality control, data normalization, data scaling,
465 dimension reduction (both linear and non-linear), clustering, differential expression analysis, batch effects
466 correction, and data visualization. Unwanted cells were removed according to the number of detectable
467 genes (number of genes <200 or >2500 were removed) and percentage of mitochondrial genes for each
468 cell. A soft threshold of percentage of mitochondrial genes was set to the 95th percentile of the current
469 dataset distribution, and the soft threshold was subject to a sealing point of 10% as the maximum threshold
470 in the case of particularly poor cell quality. Transcriptome data were normalized by a log-transform
471 function with a scaling factor of 10,000 whereas cell surface protein and antigen probe were normalized
472 by a centered log-ratio (CLR) normalization. We used variable genes in principal component analysis
473 (PCA) and used the top 15 principal components (PCs) in non-linear dimension reduction and clustering.
474 High-quality cells were then clustered by Louvain algorithm implemented in Seurat under the resolution
475 of 0.6. Differentially expressed genes for each cell cluster were identified using a Wilcoxon rank-sum test
476 implemented in Seurat. Batch effects correction analysis was performed using an Anchor method
477 implemented in Seurat to remove batch effects across different datasets. All computational analyses were
478 performed in R (version 3.6.3).

479

480 **Trajectory and pseudotime analyses**

481 Trajectory analyses were performed using Monocle 3 (version 0.2.2)^{35,36}, Seurat 3, and the
482 SeuratWrappers package (version 0.2.0)³⁷. Cells from multiple subjects were integrated to remove batch
483 effects using Seurat, and all cells were clustered into two non-connected partitions. We then performed
484 trajectory analysis on the main partition containing the majority of the cells and clusters (clusters 0–11).
485 Pseudotime analysis of cells was also inferred from this major partition using Monocle3. The root node
486 of the pseudotime analysis was set to cluster 2, a naïve B cell subset with the lowest degree of VH gene
487 SHM and CSR.

488
489 **Selection of antibodies for mAb synthesis**

490 Representative antibodies from each subject were chosen for synthesis by choosing random samplings of
491 B cells that bound to a given antigen probe with higher intensity relative to all other probes. B cells with
492 varying ranges of probe-binding intensities were chosen for confirmation by ELISA. B cells binding to all
493 probes in a polyreactive manner were also chosen and validated for polyreactivity by polyreactivity ELISA
494 (see methods below).

495
496 **Monoclonal antibody generation**

497 Immunoglobulin heavy and light chain genes were obtained by 10X Genomics VDJ sequencing analysis
498 and monoclonal antibodies (mAbs) were synthesized by Integrated DNA Technologies. Cloning,
499 transfection, and mAb purification have been previously described³⁸. Briefly, sequences were cloned into
500 human IgG1 expression vectors using Gibson assembly, and heavy and light genes were co-transfected
501 into 293T cells (Thermo Fisher). Secreted mAbs were then purified from the supernatant using protein A
502 agarose beads (Thermo Fisher).

503
504 **Enzyme-linked immunosorbent assay (ELISA)**

505 High-protein binding microtiter plates (Costar) were coated with recombinant SARS-CoV-2 proteins at 2
506 µg/ml in 1X PBS overnight at 4°C. Plates were washed the next morning with 1X PBS 0.05% Tween and
507 blocked with 1X PBS containing 20% fetal bovine serum (FBS) for 1 hour at 37°C. Antibodies were then
508 serially diluted 1:3 starting at 10 µg/ml and incubated for 1 hour at 37°C. Horseradish peroxidase (HRP)-
509 conjugated goat anti-human IgG antibody diluted 1:1000 (Jackson Immuno Research) was used to detect
510 binding of mAbs, and plates were subsequently developed with Super Aquablue ELISA substrate
511 (eBiosciences). Absorbance was measured at 405 nm on a microplate spectrophotometer (BioRad). To

512 standardize the assays, control antibodies with known binding characteristics were included on each plate
513 and the plates were developed when the absorbance of the control reached 3.0 OD₄₀₅ units. All experiments
514 were performed in duplicate 2–3 times.

515
516 **Polyreactivity ELISA**

517 Polyreactivity ELISAs were performed as previously described^{39,40}. High-protein binding microtiter plates
518 (Costar) were coated with 10 µg/ml calf thymus dsDNA (Thermo Fisher), 2 µg/ml Salmonella enterica
519 serovar Typhimurium flagellin (Invitrogen), 5 µg/ml human insulin (Sigma-Aldrich), 10 µg/ml KLH
520 (Invitrogen), and 10 µg/ml Escherichia coli LPS (Sigma-Aldrich) in 1X PBS. Plates were coated with 10
521 µg/ml cardiolipin in 100% ethanol and allowed to dry overnight. Plates were washed with water and
522 blocked with 1X PBS/0.05%Tween/1mM EDTA. MAbs were diluted 1 µg/ml in PBS and serially diluted
523 4-fold, and added to plates for 1.5 hours. Goat anti-human IgG-HRP (Jackson Immunoresearch) was
524 diluted 1:2000 in PBS/0.05%Tween/1mM EDTA and added to plates for 1 hour. Plates were developed
525 with Super Aquablue ELISA substrate (eBioscience) until the positive control mAb, 3H9⁴¹, reached an
526 OD₄₀₅ of 3. All experiments were performed in duplicate.

527
528 **Memory B cell stimulations and enzyme-linked immunospot assays (ELISpot)**

529 MBC stimulations were performed on PBMCs collected from subjects in the convalescent cohort. To
530 induce MBC differentiation into antibody secreting cells, 1x10⁶ PBMCs were stimulated with 10 ng/ml
531 Lectin Pokeweed Mitogen (Sigma-Aldrich), 1/100,000 Protein A from *Staphylococcus aureus*, Cowan
532 Strain (Sigma-Aldrich), and 6 µg/ml CpG (Invitrogen) in complete RPMI in an incubator at 37°C/5% CO₂
533 for 5 days. After stimulation, cells were counted and added to ELISpot white polystyrene plates (Thermo
534 Fisher) coated with 4 µg/ml of SARS-CoV-2 spike that were blocked with 200 µl of complete RPMI.
535 ELISpot plates were incubated with cells for 16 hours overnight in an incubator at 37°C/5% CO₂. After
536 the overnight incubation, plates were washed and incubated with anti-IgG-biotin and/or anti-IgA-biotin
537 (Mabtech) for 2 hours at room temperature. After secondary antibody incubation, plates were washed and
538 incubated with streptavidin-alkaline phosphatase (Southern Biotech) for 2 hours at room temperature.
539 Plates were washed and developed with NBT/BCIP (Thermo Fisher Scientific) for 2–10 minutes, and
540 reactions were stopped by washing plates with distilled water and allowed to dry overnight before
541 counting. Images were captured with Immunocapture 6.4 software (Cellular Technology Ltd.), and spots
542 were manually counted.

543 **Neutralization assay**

544 The SARS-CoV-2/UW-001/Human/2020/Wisconsin (UW-001) virus was isolated from a mild case in
545 February 2020 and used to assess neutralization ability of mAbs. Virus (~500 plaque-forming units) was
546 incubated with each mAb at a final concentration of 10 µg/ml. After a 30-minute incubation at 37°C, the
547 virus/antibody mixture was used to inoculate Vero E6/TMPRSS2 cells seeded a day prior at 200,000 cells
548 per well of a TC12 plate. After 30 minutes at 37°C, cells were washed three times to remove any unbound
549 virus, and media containing antibody (10 µg/ml) was added back to each well. Two days after inoculation,
550 cell culture supernatant was harvested and stored at -80°C until needed. A non-relevant Ebola virus GP
551 mAb and PBS were used as controls.

552
553 To determine the amount of virus in the cell culture supernatant of each well, a standard plaque-forming
554 assay was performed. Confluent Vero E6/TMPRSS2 cells in a TC12 plate were infected with supernatant
555 (undiluted, 10-fold dilutions from 10⁻¹ to 10⁻⁵) for 30 minutes at 37°C. After the incubation, cells were
556 washed three times to remove unbound virus and 1.0% methylcellulose media was added over the cells.
557 After an incubation of three days at 37°C, the cells were fixed and stained with crystal violet solution in
558 order to count the number plaques at each dilution and determine virus concentration given as plaque-
559 forming units (PFU)/ml. A stringent cutoff for neutralization was chosen as 100-fold greater neutralization
560 relative to the negative control mAb.

561
562 **Statistical analysis**

563 All statistical analyses were performed using Prism software (GraphPad Version 7.0). Sample sizes (n)
564 are indicated directly in the figures or in the corresponding figure legends and specific tests for statistical
565 significance used are indicated in the corresponding figure legends. P values less than or equal to 0.05
566 were considered significant. *p<0.05, **p<0.01, ***p<0.001, ****p<0.0001.

567
568 **Data Availability**

569 The single B cell dataset generated during this study is available from the corresponding author on
570 reasonable request or upon publication.

571

572

573

574

575 **Acknowledgements**

576 We kindly thank the Joachimiak, Fremont, and Krammer laboratories for providing recombinant antigens
577 for our sorting experiments. We thank Dr. Maria Lucia Madariaga for organizing the COVID-19
578 convalescent cohort study and Maud O. Jansen for coordinating blood donor visits and delivering samples.
579 We thank Dr. Nicholas Chevrier for graciously allowing us to use the Pritzker School of Molecular
580 Engineering's sequencing facility. We are thankful to Dr. Steven A. Erickson for thoughtful suggestions
581 and discussion, and Dr. Linda Yu-Ling Lan for providing the initial framework for the oligo-tagged
582 antigen-bait sorting approach. Lastly, we are grateful to the patients who donated samples for our research
583 purposes upon recovery from COVID-19.

584
585 **Funding**

586 This project was funded in part by the National Institute of Allergy and Infectious Disease (NIAID);
587 National Institutes of Health (NIH) grant numbers U19AI082724 (P.C.W.), U19AI109946 (P.C.W.),
588 U19AI057266 (P.C.W.), the NIAID Centers of Excellence for Influenza Research and Surveillance
589 (CEIRS) grant numbers HHSN272201400005C (P.C.W.). N.W.A. was supported by the Multi-
590 disciplinary Training program in Cancer Research (MTCR) - NIH T32 CA009594. A.J. and R.P.J were
591 supported by federal funds from the NIAID, NIH, and Department of Health and Human Services under
592 Contract HHSN272201700060C. F.K and F.A. were funded by the NIAID CEIRS contract
593 HHSN272201400008C, Collaborative Influenza Vaccine Innovation Centers (CIVIC) contract
594 75N93019C00051 and the generous support of the JPB foundation, the Open Philanthropy Project (#2020-
595 215611) and other philanthropic donations. Y.K. and P.H. were funded by the Research Program on
596 Emerging and Re-emerging Infectious Disease grant (JP19fk0108113) and the Japan Program for
597 Infectious Diseases Research and Infrastructure (JP20fk0108272) from the Japan Agency for Medical
598 Research and Development (AMED), NIAID CEIRS contract HHSN272201400008C, and CIVIC
599 contract 75N93019C00051. D.F., C.N, Y.D., and P.D.H, were supported by NIAID contracts
600 HHSN272201700060C and 75N93019C00062.

601
602 **Author Contributions**

603 C.S. and H.L.D. collected samples, designed and performed experiments, analyzed the data, and wrote the
604 manuscript. L.L. performed computational analyses of single cell data and wrote the manuscript. N.W.A.
605 generated VDJ, 5' transcriptome and feature libraries, and performed Illumina sequencing. P.J.H.
606 performed virus neutralization assays with mAbs. N.-Y.Z. collected samples, expressed recombinant

607 SARS-CoV-2 proteins, and generated mAbs. M.H. performed mAb cloning. J.J.G. collected samples and
608 performed ELISpots and serum ELISAs, O.S. and J.W. performed serum ELISAs, and J.W. assisted in
609 mAb generation. M.L.M., K.S., and M.O.J. coordinated the convalescent COVID-19 clinical study and
610 collected patient samples. I.S. performed ELISAs. S.C. collected samples, performed ELISAs, and
611 expressed recombinant SARS-CoV-2 proteins. H.A.U. collected samples and expressed recombinant
612 SARS-Cov-2 proteins. J.H. provided funding and resources for N.W.A. to perform sequencing. F.A., C.N.,
613 Y.-N.D., P.D.H., D.F., R.P.J., A.J., and F.K. provided recombinant SARS-CoV-2 proteins. Y.K. provided
614 mAb neutralization data. P.C.W. supervised the work, analyzed the data, and wrote the manuscript.

615

616 **Competing Interests**

617 NowDiagnostics (Springdale, Arkansas) is investigating the use of monoclonal antibodies generated from
618 this study for the development of diagnostic tests.

619

620

621

622

623

624

625

626

627

628

629

630

631

632

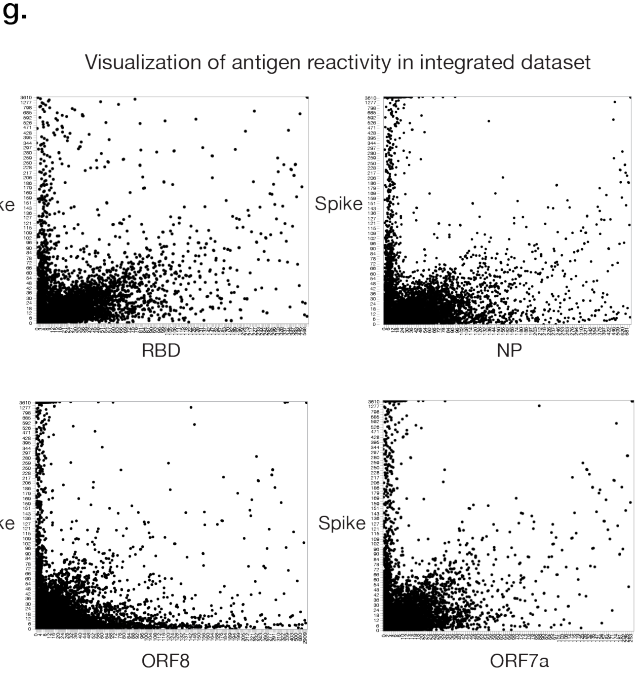
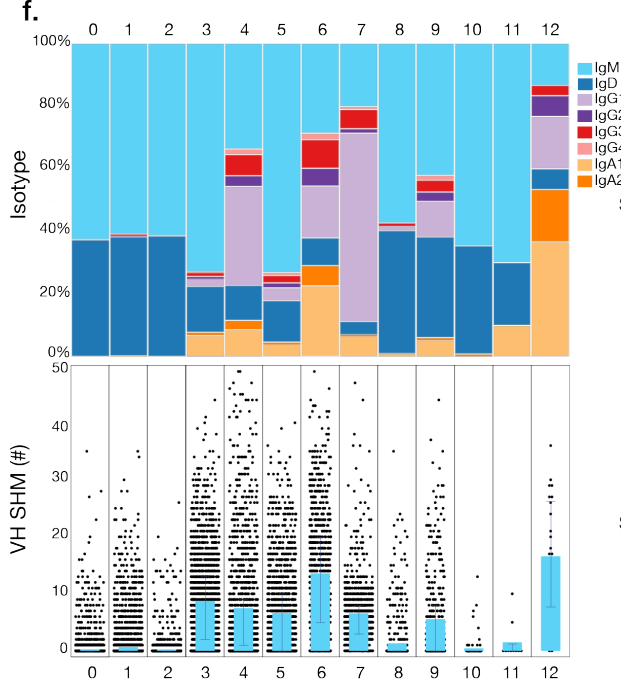
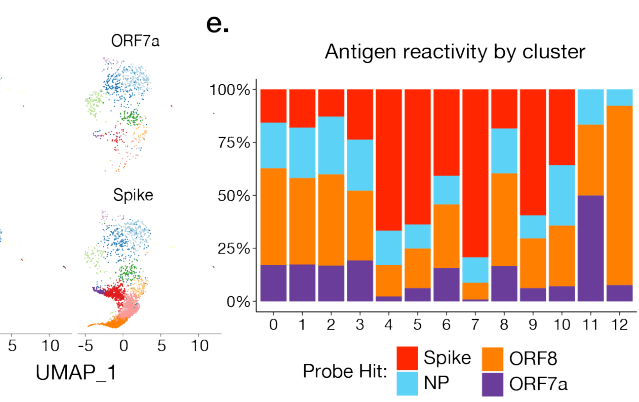
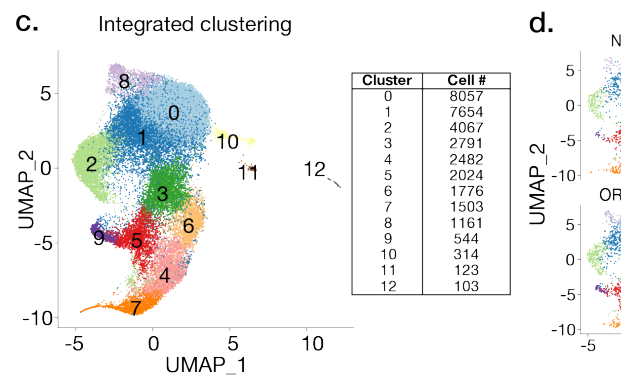
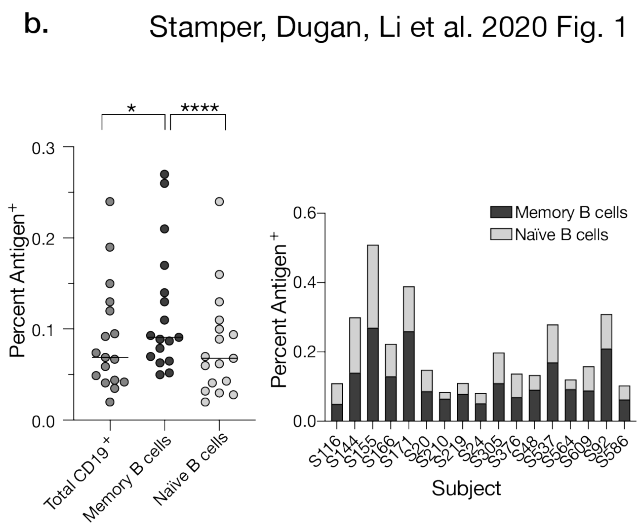
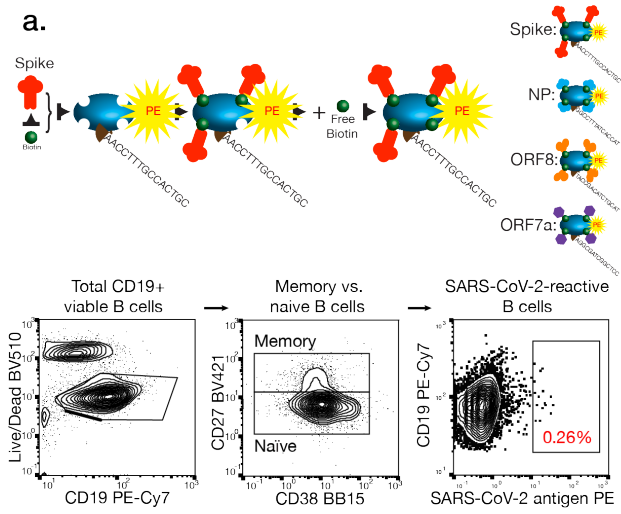
633

634

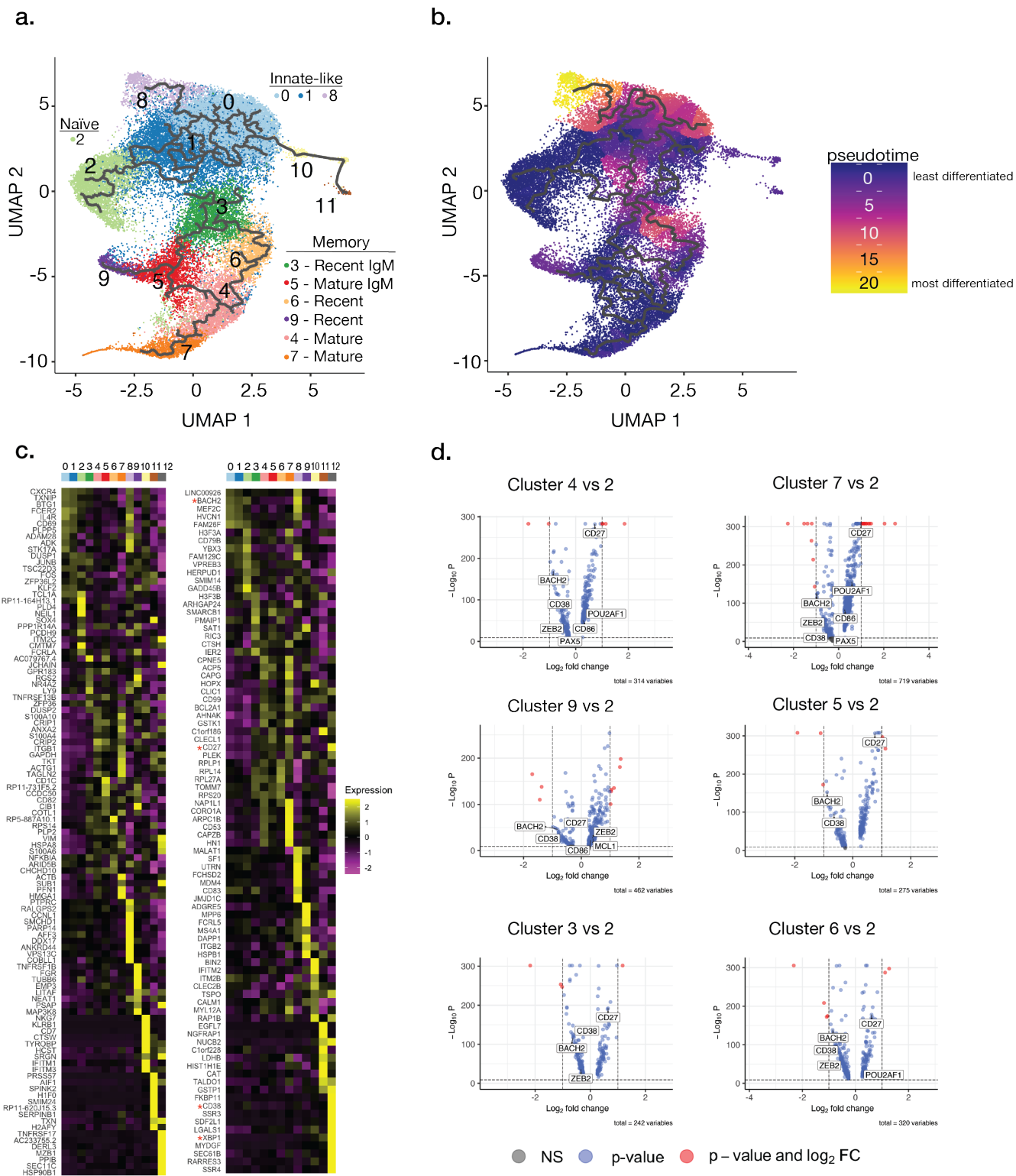
635

636

637

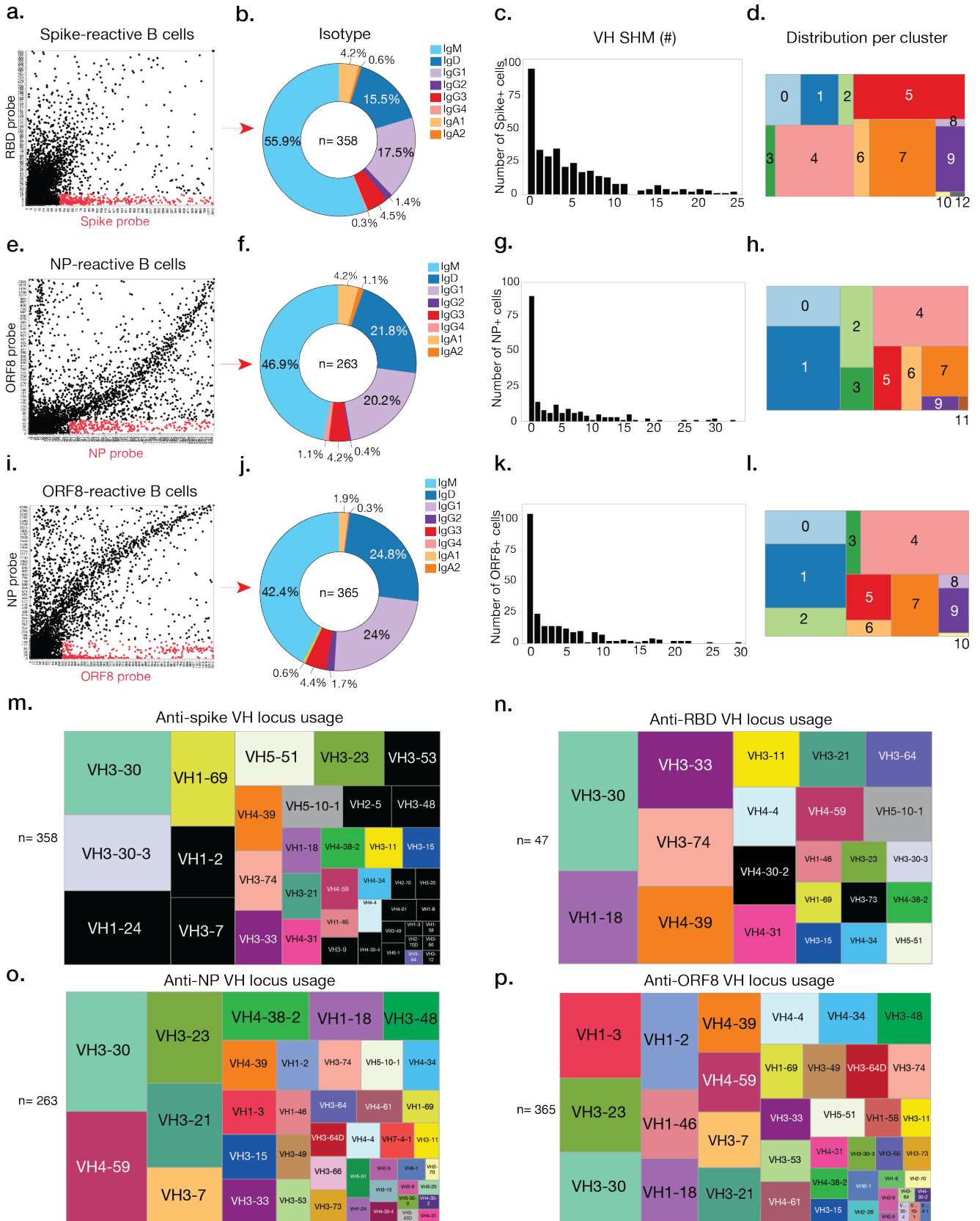


640 **Fig. 1: B cell subsets enriched for SARS-CoV-2-reactivity are revealed by transcriptome, Ig**
641 **repertoire, and probe binding. a**, Model demonstrating antigen probe preparation and representative
642 gating strategy for sorting antigen-positive B cells. **b**, Percentage of antigen-probe-positive total B cells
643 (CD19⁺CD3⁻), naïve B cells (CD27⁺CD37^{int}), and memory B cells (CD27⁺CD38^{int}) (left), and naïve vs.
644 memory B cells by subject (right; n=17 subjects). Statistics are paired non-parametric Friedman test
645 (*p=0.0491; ****p<0.0001). **c**, Integrated transcriptional UMAP analysis of distinct B cell clusters and
646 the corresponding number of B cells per cluster. **d**, Feature library enrichment of antigen-probe-positive
647 B cells by cluster. **e**, Percent probe reactivity of all B cells by cluster. **f**, Ig isotype usage and VH gene
648 SHM for all antigen-positive B cells per cluster. Bars indicate median with interquartile range. **g**,
649 Representative visualization of antigen reactivity revealing antigen-specific B cells. Axes indicate antigen
650 probe intensities.
651



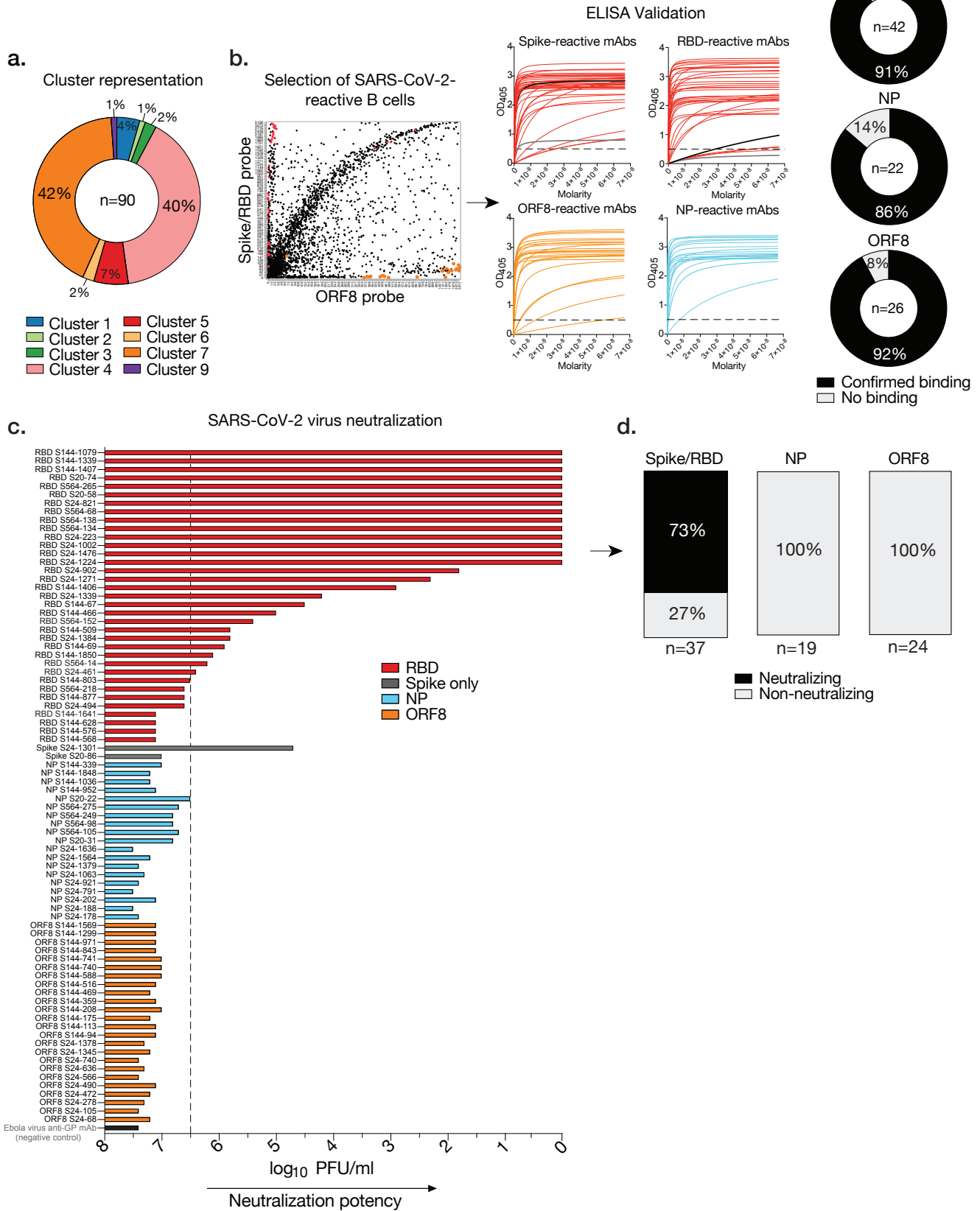
654 **Fig. 2: Transcriptional analysis distinguishes naïve, innate-like and MBC subsets specific to**
655 **SARS-CoV-2 proteins. a–b**, Trajectory (**a**) and pseudotime (**b**) analyses of clusters 0–11 reveals least
656 to most differentiated clusters. Cluster 12 is excluded from trajectory analysis as it represents a separate
657 partition as defined by Monocle3. **c**, Heatmap showing the top twenty most differentially expressed
658 genes per cluster. Red stars denote genes used in memory B cell (MBC) identification. **d**, Volcano plots
659 comparing differentially expressed genes in MBC-like clusters relative to cluster 2 (naïve B cells).
660 Genes used in MBC identification are indicated: *cd27*, *cd38*, *hhex*, *zeb2*, *pou2af1*, *spib*, *cd80*, *cd86*,
661 *mcl1*, *prdm1*, *abp1*, *manf*, *bach2*, *pax5*. Red-colored dots represent a log fold change in expression >0.1
662 and an adj-p value <0.01. Putative B cell subset identities are highlighted where they could be clearly
663 defined (**a**).

664

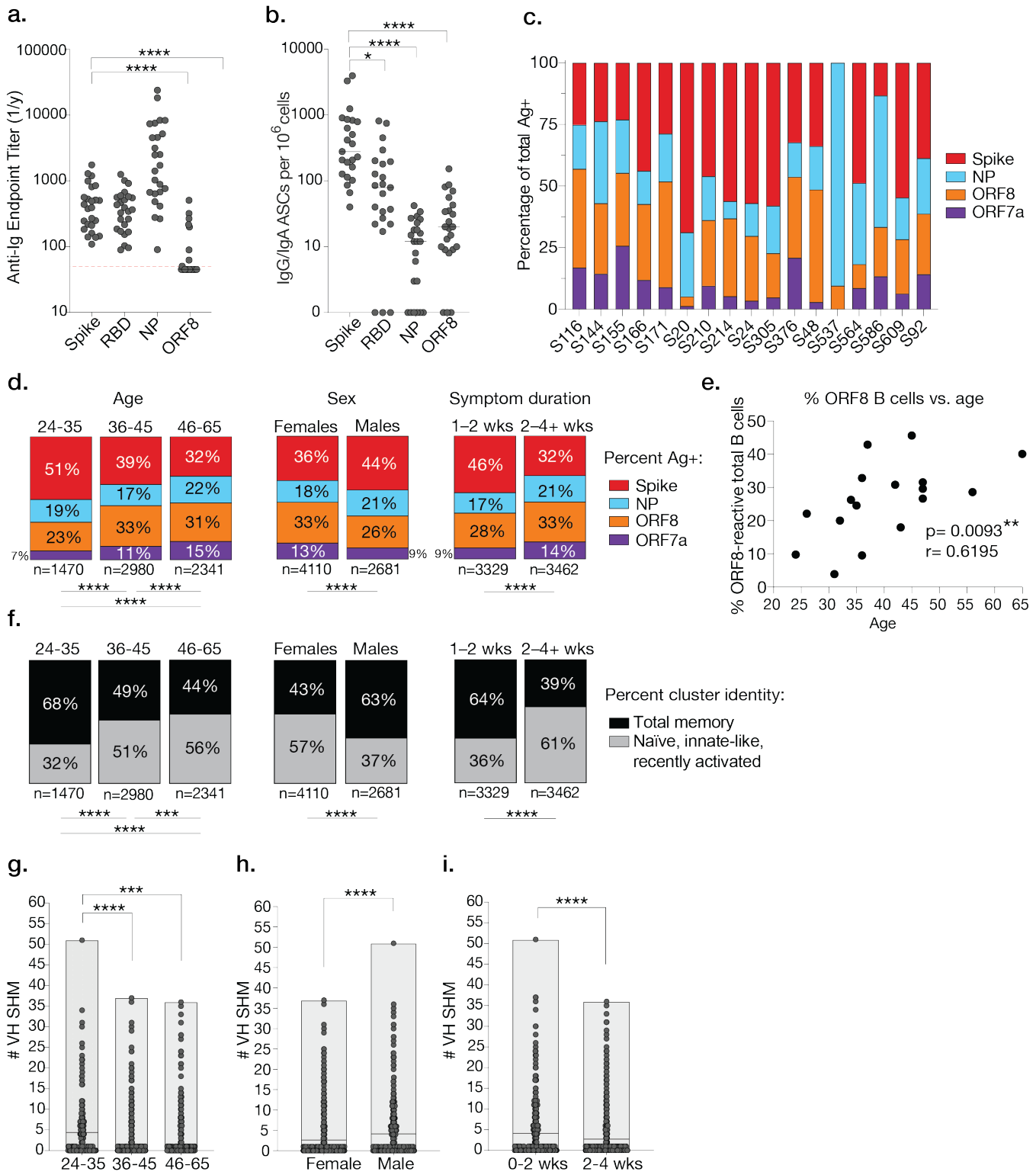


666 **Fig. 3: SARS-CoV-2-reactive B cells exhibit unique features for isotype, SHM, subset of origin, and**
667 **VH gene usage. a–l**, Ig isotype, VH gene SHM, and distribution of B cells by integrated cluster for spike-
668 **(a, b, c, d)**, NP- **(e, f, g, h)** and ORF8-specific B cells **(i, j, k, l)**. **m–p**, Tree maps showing frequency of
669 VH gene locus usage for total spike (including RBD) **(m)**, RBD only **(n)**, NP **(o)**, and ORF8-specific B
670 cells **(p)**. Numbers in the center of each pie chart and below each tree map indicate number of cells
671 analyzed per reactivity.

Stamper, Dugan, Li et al. 2020 Fig. 4



673 **Fig. 4: Characterization of mAbs from single SARS-CoV-2-reactive B cells. a,** Cluster origin of
674 cloned mAbs (n=90). **b,** Representative plot showing the selection of B cells chosen to clone mAbs,
675 antigen binding curves by ELISA for each reactive mAb (spike, n= 38; RBD, n=36; NP, n=19; ORF8,
676 n=24), and percentages of total cloned mAbs exhibiting specificity (right). Dashed line on ELISA curves
677 represents the OD₄₀₅ cutoff of 0.5 for positivity. **c,** Neutralization potency (log₁₀ PFU/ml) of mAbs
678 tested by live SARS-CoV-2 virus plaque assay. Dashed line at x= 6.5 indicates cutoff for neutralization.
679 **d,** Percentage of total spike, NP, and ORF8-specific mAbs that displayed neutralization activity.
680 Numbers below each bar chart indicate the number of mAbs tested for neutralization. ELISA data are
681 representative of 2–3 independent experiments and mAbs were screened once for neutralization ability.
682
683
684



685

686

687

Fig. 5: B cell antigen targeting, subset distribution, and adaptability is linked to clinical features. a,

Total serum anti-Ig endpoint titers for SARS-CoV-2 antigens determined by ELISA (n=25 subjects). b,

688 Number of IgG/IgA antibody secreting cells (ASCs) per 10^6 cells determined by ELISpot (n=23 subjects).
689 **c.** Percentage of antigen-probe-positive cells by subject. **d.** Percentage of antigen-probe-positive cells
690 stratified by age (in years), sex, and symptom duration (in weeks). **e.** Spearman correlation between
691 percentage of all cells specific to ORF8 and subject age with p and r values indicated. **f.** Percentage of
692 antigen probe positive B cells in MBC-like clusters (3, 4, 5, 6, 7, 9, and 12) or naïve and innate-like
693 clusters (0, 1, 2, 8, 10, 11) stratified by age, sex, and symptom duration. **(g–i)** VH gene SHM for antigen-
694 specific cells from a given age (**g**), sex (**h**), or symptom duration group (**i**). Data in **a** and **b** were analyzed
695 using paired non-parametric Friedman tests with multiple comparisons against the spike (*p=0.0154,
696 ****p<0.0001). Red dashed line in **a** at y=45 indicates cutoff for no serum titer detected. The data in **d**
697 and **f** were analyzed using Chi-square or Fisher’s exact tests, (****p<0.0001; ***p=0.0009). Data in **g**
698 were analyzed using unpaired non-parametric Kruskal Wallis (****p<0.0001; ***p=0.0002). Statistics
699 used in **h** and **i** are unpaired non-parametric Mann-Whitney tests (****p<0.0001).

700

701

702

703

704

705

706

707

708

709

710

711

712

713

714

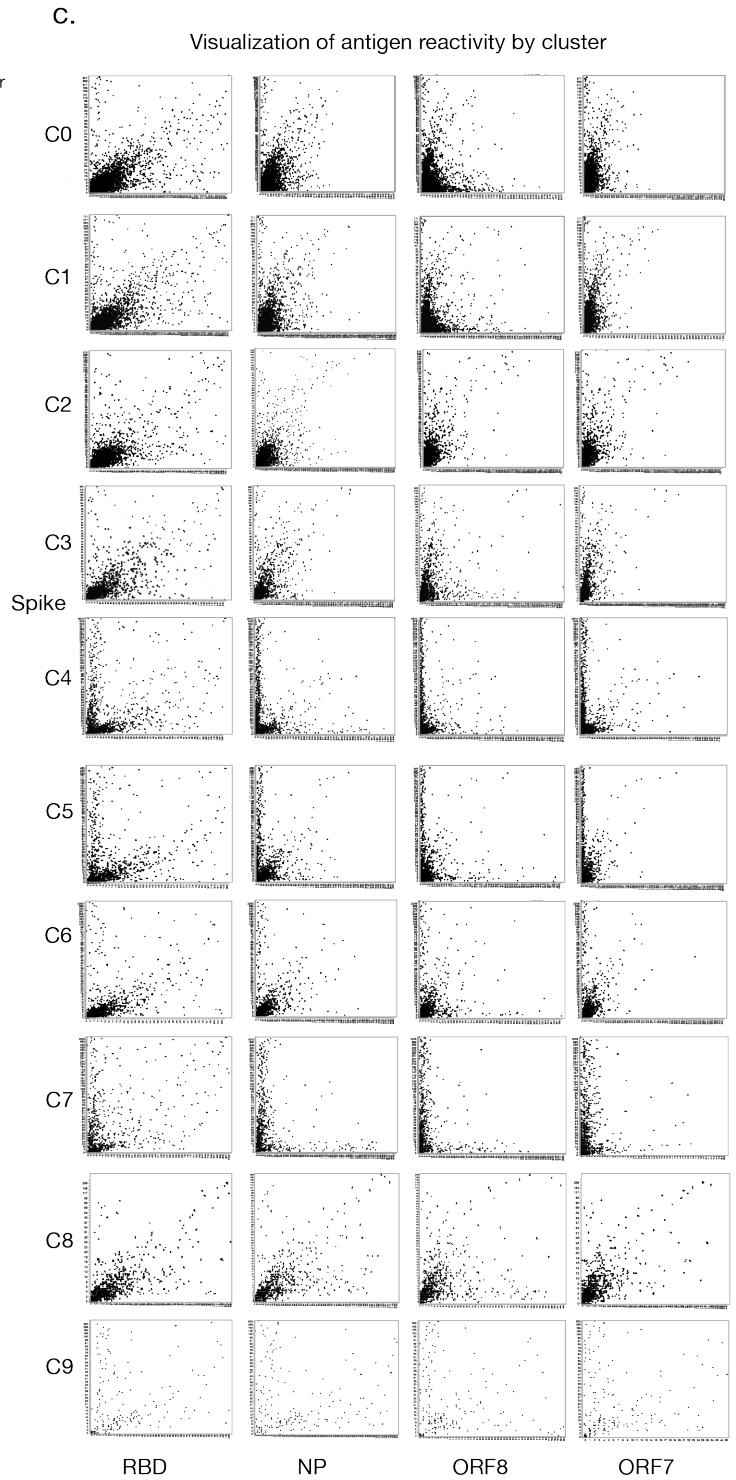
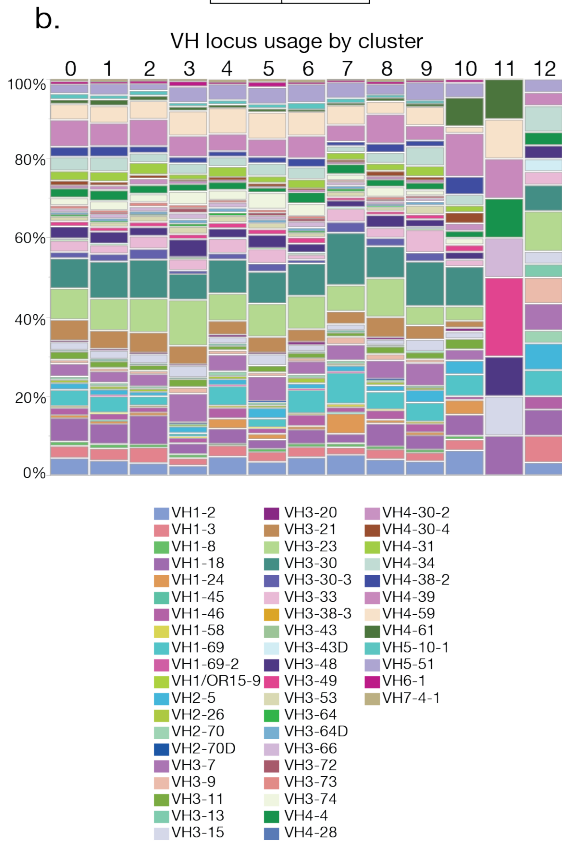
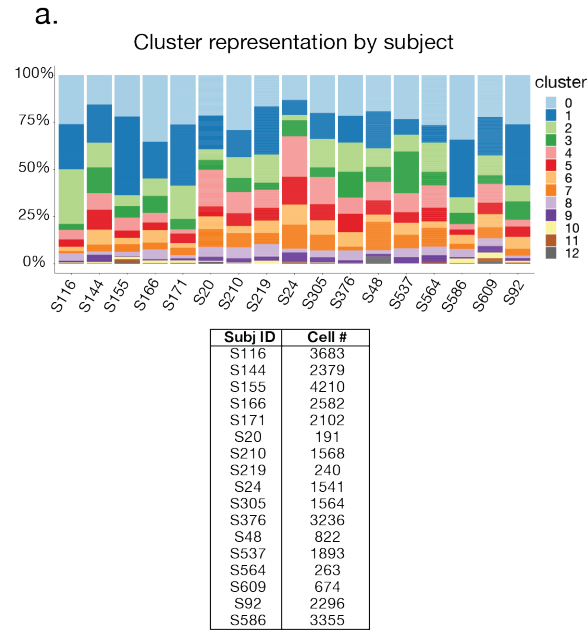
715

716

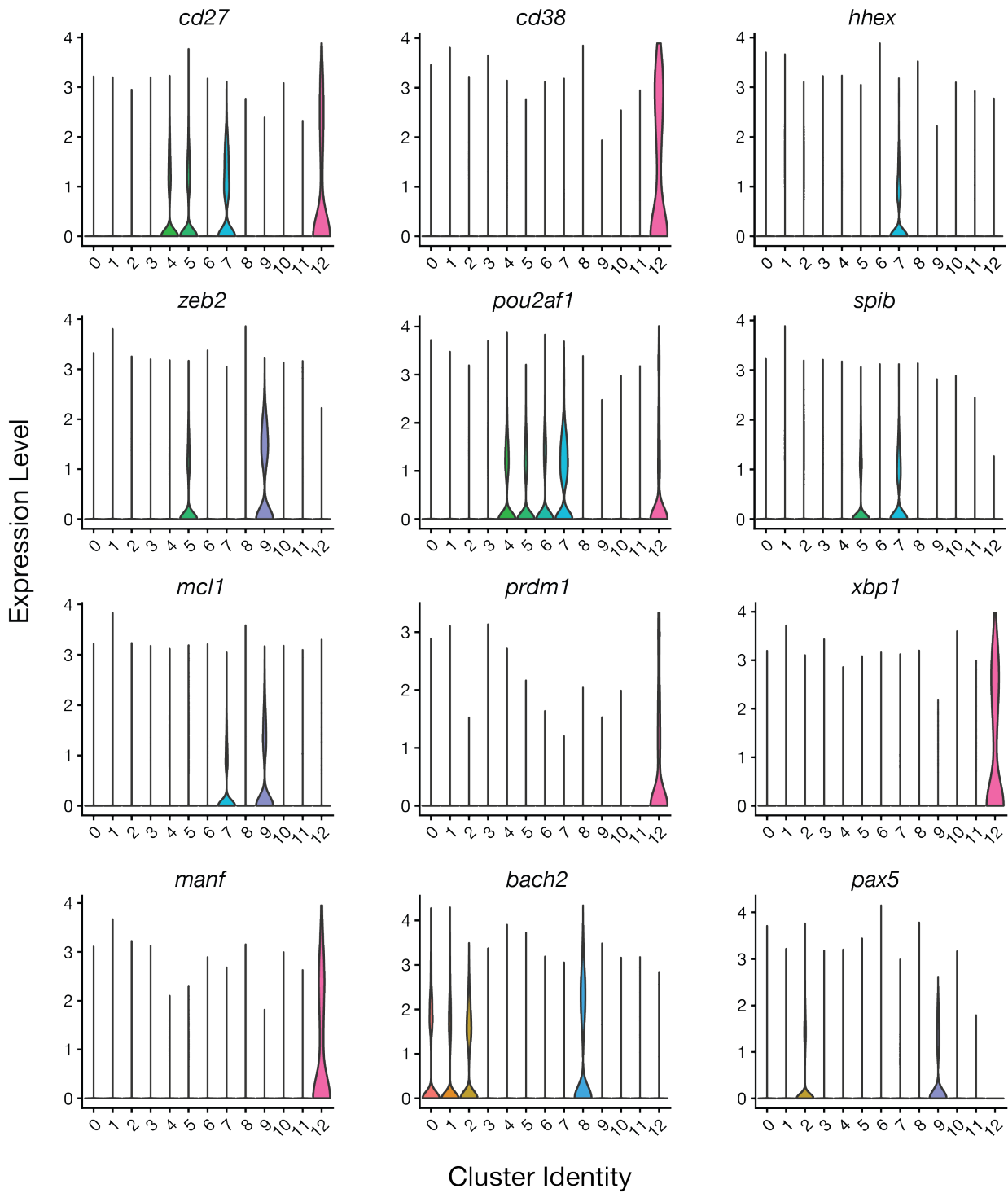
717

718

719



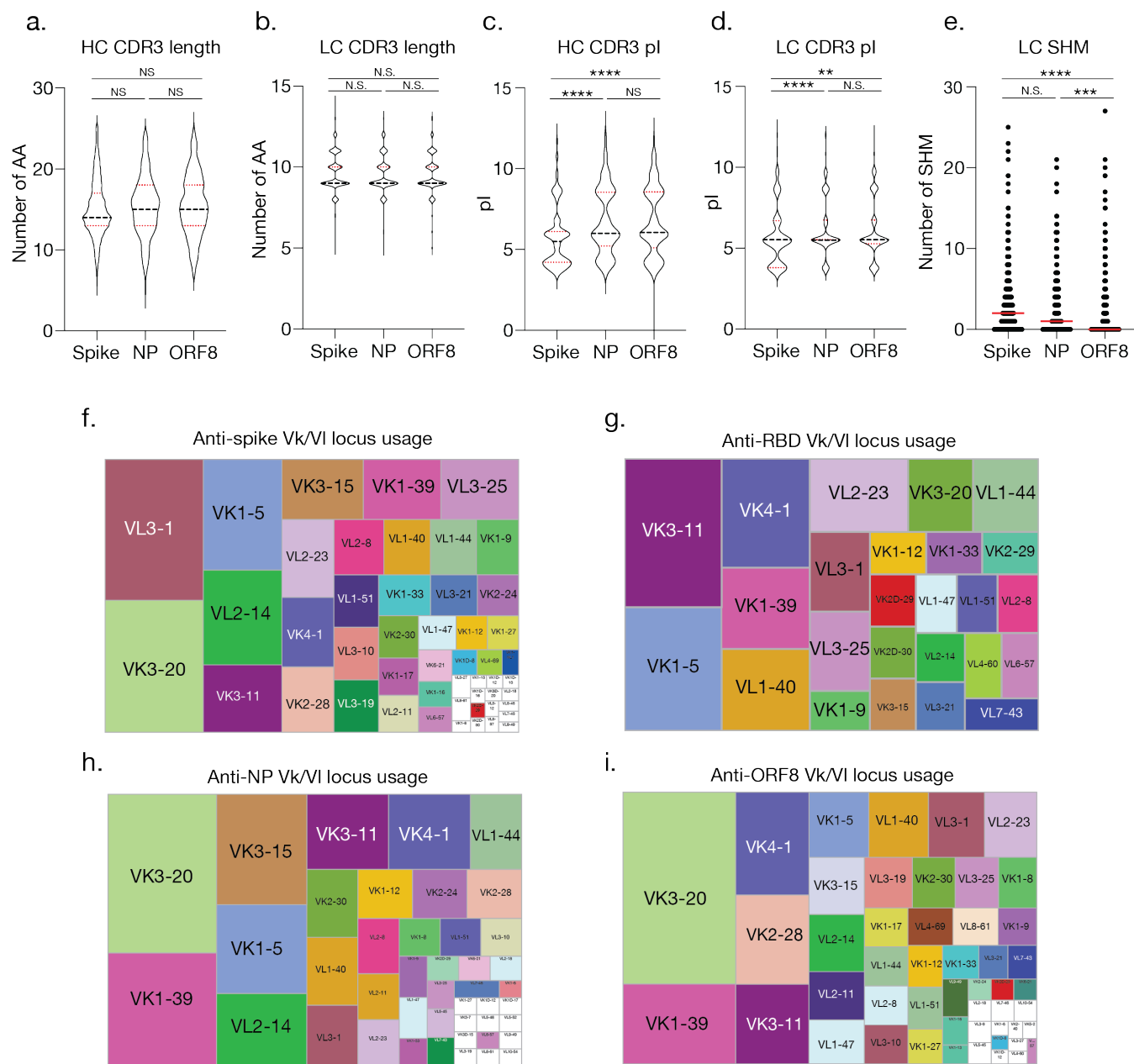
722 **Extended Data Fig. 1. Additional characteristics of B cells comprising integrated clusters. a,**
723 Antigen-probe-positive B cell distribution across integrated clusters by subject with the number of cells
724 per subject indicated. **b,** Variable gene segment usage in B cell receptor heavy chains of antigen-probe-
725 positive B cells across integrated clusters. **c,** Diagrams showing antigen-probe-positive B cells per
726 cluster with probe intensities for the indicated antigens plotted on the axes.



727

728 **Extended Data Fig. 2. Expression of MBC and LLPC gene markers in integrated clusters.**

729 Normalized expression levels of the indicated genes represented as violin plots.



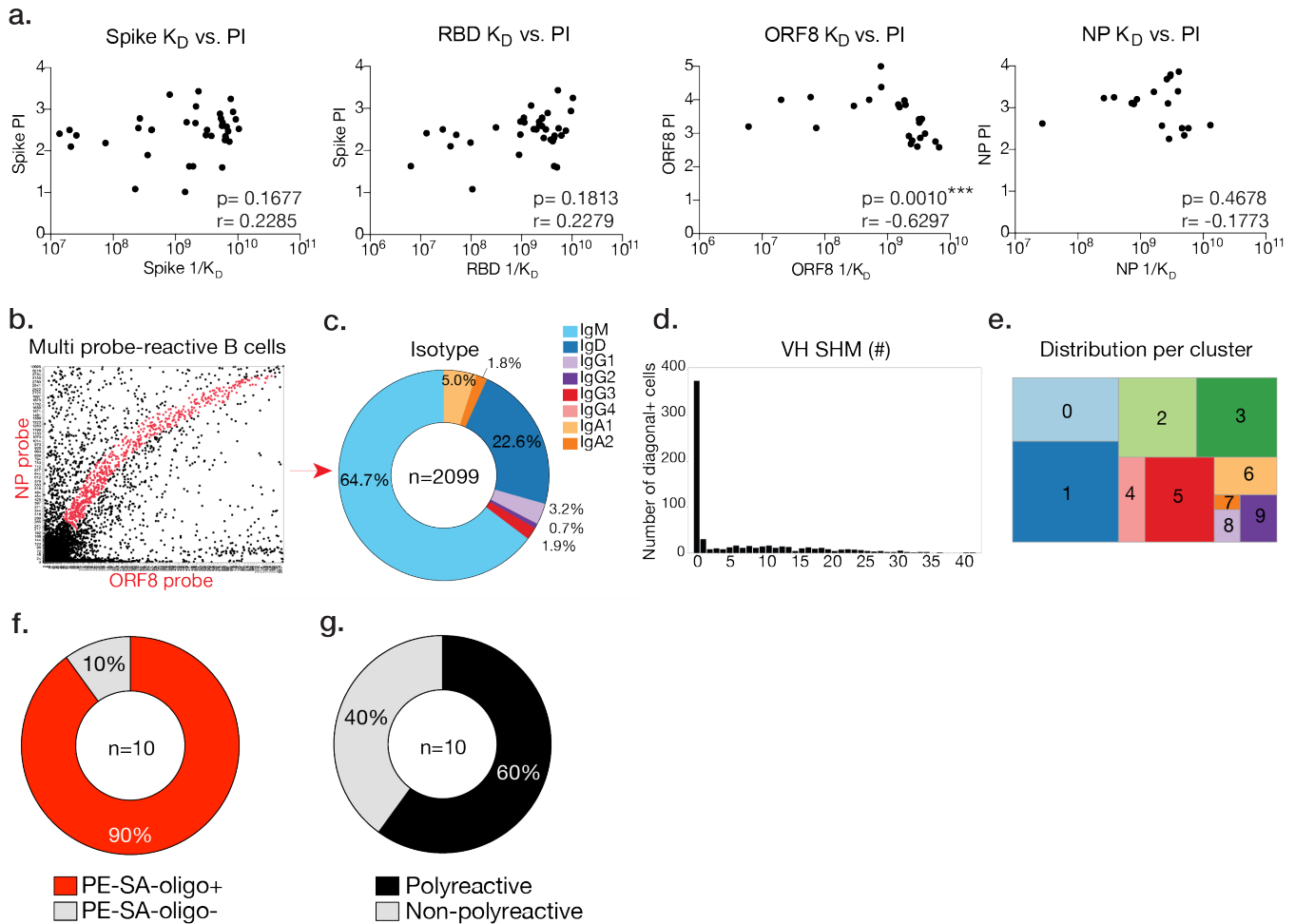
730
731

732 **Extended Data Fig. 3. Heavy and light chain features of SARS-CoV-2 reactive B cells. a–b,** Heavy
733 chain (HC, **a**) and light chain (LC, **b**) complementarity determining region 3 (CDR3) lengths, shown by
734 antigen-reactivity. **c–d,** HC (**c**) and LC (**d**) isoelectric points pI, shown by antigen-reactivity. **e,** Number
735 of light chain (LC) somatic hypermutations (SHM), shown by antigen-reactivity. **f–i.** Tree maps showing
736 frequency of Vk/L gene locus usage for spike- (**f**), RBD- (**g**), NP- (**h**), and ORF8-specific B cells (**i**). In
737 panels **a–e** groups were compared by Kruskal-Wallis test (N.S.= not significant, ****p<0.0001;

738 ***p=0.0006; **p=0.0033). For f-i, n=531 for spike, n=47 for RBD, n=293 for NP, and n=463 cells
 739 selected for ORF8.

740

Stamper, Dugan, Li et al. 2020 Extended Data Fig. 4



741

742 **Extended Data Fig. 4. Additional features of mAbs cloned from antigen-specific and multi-probe**
 743 **binding B cells.** **a**, ELISA K_D for specific mAbs against the spike, RBD, ORF8, and NP, versus
 744 normalized probe intensity for spike, ORF8, and NP respectively. Whole spike antigen probe intensities
 745 are plotted for RBD-binding mAbs. Statistics are Spearman correlations with p and r values indicated. **b**,
 746 Example selection of multi-probe-reactive B cells. **c**, Isotype frequencies of multi-probe-reactive B cells.
 747 **d**, Number of VH gene SHM for multi-probe-reactive B cells. **e**, Proportion of multi-probe-reactive B
 748 cells in integrated clusters. **f**, Percentage of multi-probe-reactive B cells binding PE-SA-oligo by ELISA.
 749 **g**, Percent multi-probe-reactive B cells exhibiting polyreactivity, as determined by ELISA. Numbers in
 750 the center of each pie chart indicate number of B cells/mAbs analyzed.

751 **Extended Data Tables**

752 **Extended Data Table 1.** Individual patient information.

753 **Extended Data Table 2.** Distribution of clinical parameters for patients included in the study.

754 **Extended Data Table 3.** MAbs generated from single B cell heavy and light chain gene sequences.

755 **Extended Data Table 4.** Public B cell clones identified from the integrated single cell sequencing
756 dataset.